

7th CIRP Conference on Surface Integrity

Simulative and experimental investigation of the surface integrity obtained by Non-Circular-Rotary-Turning (NCRT)

Tassilo Arndt^{*a}, Volker Schulze^a

^awbk Institute of Production Science, Karlsruhe Institute of Technology (KIT), Kaiserstr. 12, 76131 Karlsruhe, Germany

^{*}Corresponding author. Tel.: +49-721-608-42455; fax: +49-721-608-45004. E-mail address: tassilo.arndt@kit.edu

Abstract

Components with non-circular contours are increasingly used in technical applications, for example in shaft-hub connections or for medical implants with bionic-induced contours. A novel process approach for the production of these contours is the Non-Circular-Rotary-Turning (NCRT). The technology is based on the principle of kinematic coupling of workpiece and tool rotation, which allows to transfer the non-circular shape of the tool to the component within certain limits. All linear axes except the feed axis are not in motion during this process. In contrast to conventional turning, the non-circular contour and the complex kinematics of NCRT lead to surfaces that are strongly depending on the measuring position on the component. In this work, the surfaces obtainable by NCRT are generally investigated. Using an example cross section, a kinematic dexel-based simulation is utilized to predict the kinematic surface topography depending on the process parameters. The surfaces are also investigated in experiments and compared with the simulation. The results show a characteristic surface topography, as well as a strong dependence on the ratio of tool to workpiece diameter. Better surfaces are generally achieved in downturning.

© 2024 The Authors. Published by Elsevier B.V.

This is an open access article under the CC BY-NC-ND license (<https://creativecommons.org/licenses/by-nc-nd/4.0>)

Peer-review under responsibility of the scientific committee of the 7th CIRP Conference on Surface Integrity

Keywords: non-circular contours; kinematic simulation; synchronized-cyclic processes; Non-Circular-Rotary-Turning (NCRT)

1. Introduction

Components with non-circular contours are used in a wide variety of technical fields. Typical areas of application range from cams and camshafts in automotive industry to form fitting shaft-hub connections in drive technology or tool interfaces in machine tools. Curved contours with non-circular or rectangular cross-sections can also be found in medical applications e.g. bionic-inspired implants. However, non-circular contours are often a challenge for economical production, as they typically involve multi-stage process chains consisting of e.g. turning, milling and grinding.

New and promising manufacturing processes such as polygon turning enable the production of polygonal profiles on a lathe with high productivity and accuracy [1]. Internal and external profiles can be produced in the same kinematics, which is why this process is especially interesting for manufacturing shaft-hub connections [2]. From a geometrical point of view, only hypocycloidal profiles can be produced [3].

Nomenclature

d_{a0}	Tip diameter of the tool
d_{a2}	Diameter of circumscribed circle of the workpiece
d_{i2}	Diameter of inscribed circle of the workpiece
d_{r2}	Diameter of reference circle of the workpiece
d_R	Balk diameter of the workpiece
f	Feed rate
h_{\max}	Maximum chip thickness
i	Transmission ratio
v_c	Cutting speed
v_t	Rotation speed of the tool
ζ	Angle of cutting traces
Σ	Axis crossing angle
ω_0	Angular velocity of the tool
ω_2	Angular velocity of the workpiece

Much greater geometrical freedom is available with the non-circular turning process (NCTP). Here, the cutting tool is moved by a fast tool servo synchronized with the spindle rotation to create the non-circular contour of the workpiece [4]. Cutting angles and feed rate vary periodically due to the nature of the process, which can have an unfavorable effect on the part geometry and surface quality [5]. This can be partially remedied with suitable process strategies such as reducing chatter vibration by continuous variation of the spindle speed in the process [6]. On the other hand, part quality and productivity are strongly dependent on the characteristics of the servo, which is why a specialized machine is generally required. There is no process with multiple geometric degrees of freedom that can be implemented in existing lathes.

In this work, the novel process Non-Circular-Rotary-Turning (NCRT) is presented and the surfaces obtained are generally investigated. A kinematic dixel-based simulation is utilized to predict the kinematic surface topography depending on the process parameters. In experimental investigations, the real topography of the components is determined and compared with the results of the simulation. Results reveal that the topography mainly depends on the ratio of sliding speed and cutting speed and is thus significantly dependent on the tool diameter.

1.1. Non-Circular-Rotary-Turning (NCRT)

Like gear skiving [7] or polygon turning, NCRT is a synchronized-cyclic process whose technology is based on the principle of kinematic coupling. This means, tool rotation ω_0 and workpiece rotation ω_2 are synchronized with a fixed transmission ratio i in a position-controlled manner, see equation 1. This fixed transmission ratio allows to transfer the non-circular shape of the tool to the workpiece within certain limits. Both are arranged with an axis crossing angle Σ of 90° , see figure 1. Other Σ are conceivable.

$$i = \frac{\omega_0}{\omega_2} \quad (1)$$

In contrast to NCTP, all linear axes of the machine, with exception of the feed axis, are motionless during the process. By changing the tool rotation direction, the chip thickness progression over time can be changed. Similar to milling, downmilling and upmilling chip thickness progression can be achieved. However, since NCRT is a turning process (the cutting speed results exclusively from the workpiece rotation due to $\Sigma = 90^\circ$), the modified terminology downturning (DT) and upturning (UT) is used in the following.

1.2. Surface integrity obtained with kinematically related processes

A kinematically related process to NCRT with a completely different aim is Actively-Driven-Rotary-Tool (ADRT). Here, a round driven tool insert is used to machine difficult-to-cut materials such as Inconel 718 [8]. The result is round workpieces. The process is used to extend tool life by reducing the thermal

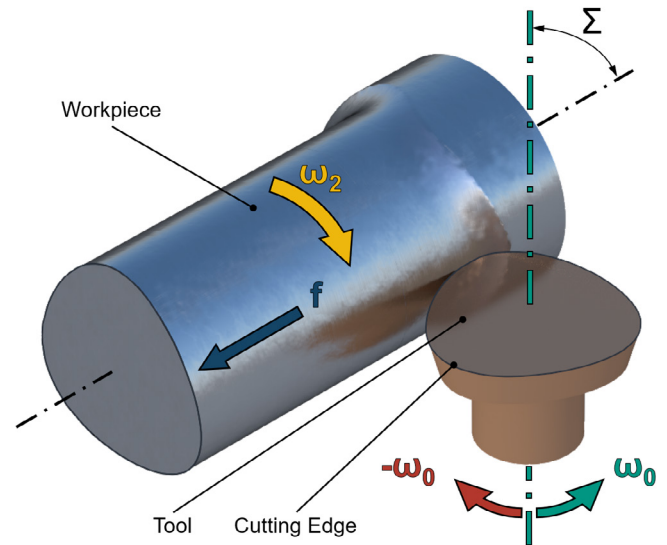


Figure 1: Basic kinematics of the Non-Circular-Rotary-Turning (NCRT). Downturning (DT) uses positive ω_0 , Upturning (UT) negative.

load on the tool as a particular part of the cutting edge is in use for a short period of time, followed by a rest period in which the cutting edge can cool down [9]. For ADRT, position-controlled synchronization between workpiece and tool is not necessary. Essential similarity between ADRT and NCRT is the high ratio of rotation speed of the tool v_t in relation to the cutting speed v_c . Therefore, a brief overview of the state of research concerning surface integrity in ADRT is given below.

Nakajima et al. [10] machine SUS 304 with a coated carbide tool at $\Sigma = 80^\circ$ and vary the tool position. The best surface is achieved with the tool in the centered position, where the rake face coincides with the perpendicular of the axes. In processes with off-centered tool position adhered chips appear on the machined surface. The authors assign this to an unfavorable influence on the chip flow direction, allowing chips to get between the tool and the workpiece. A surface topography typical for ADRT is found by Olgun & Budak [11] when machining AISI 1050 with CVD coated carbide tools. Cutting traces appear on the surface at an angle to the direction of feed motion, which the authors attribute to tool spinning. Kaulfersch & Roeder [12] found a correlation between lower surface roughness and lower process force when machining Inconel 718. Here, the surface quality of the machined parts is heavily dependent on the selected process parameters [8]. Joch et al. [13] confirm this also for machining Ti6Al4V (Titan Grade 5) in a widespread parameter study, where they varied the depth of cut, feed rate f , v_c and v_t on two levels each. Accordingly, v_c has the greatest influence on the surface quality. Chip adhesion to the machined surface occur at high v_c in combination with low v_t . The best surfaces were achieved with high f and high depth of cut. Despite this unexpected result, there is no critical discussion regarding minimum chip thickness considering the very small f and depth of cut used resulting in high surface roughness.

2. Simulation

Similar to gear skiving, the challenge of NCRT is the determination of the geometric shape of the tool depending on the desired workpiece contour and the kinematics used, as well as the choice of suitable process parameters. For this reason, the design methodology is based on the same principles according to [7]. In a first step, the geometric shape of the tool is derived from the desired contour of the workpiece using a mathematical model. In a second step, the obtained tool contour is used, for example, to calculate the actual contour of the workpiece or effective process parameters such as chip thicknesses or rake angles. Therefore OpenSkiving is chosen as a basis to develop and implement simulation models for NCRT. OpenSkiving is a MATLAB®-based Open-Source-Software to design gear skiving processes [14]. For the calculations mainly dixel-based simulation approaches are used as described in [15].

To calculate the kinematic surface topography, the shape of the tool, which is represented by discrete points, is moved in space relative to the workpiece according to the kinematics of NCRT. The resulting volume is reduced to a so-called tool helix surface to save computation time in the following steps. For this purpose, all points of the volume are removed which are further away from the Z-axis than the radius of the blank part $d_R/2$, see figure 2a). Subsequently, dixel are generated around the discrete part contour, which follow the normal vectors. This dixel blank is intersected and trimmed with the tool helix surface and the deviations are calculated for this plane at a certain Z position, see figure 2b). To obtain the kinematic topography of the workpiece, this calculation is repeated at different Z positions. Furthermore, the maximum height difference alongside the workpiece axis is calculated from the topography. For periodic surface structures, this value corresponds to the average surface roughness R_z and is referred to as $R_{z_{sim}}$ in the following to distinguish it from the experimental measured value.

The tool helix surface can also be used to calculate the contact line for NCRT: For each discrete step of the kinematics, the discrete tool point with the smallest radius around the Z axis is determined. The entirety of these points results in the contact line, see figure 2a).

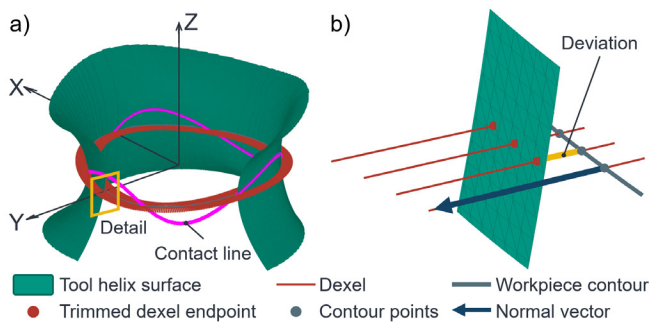


Figure 2: Simulation method to calculate kinematic surface topography and contact line: a) The tool helix surface is the reduced tool helix volume. b) Deviations are calculated using a dixel-based approach.

3. Experimental Setup

A hypocycloidal profile [16] with three tappets and parameters according to table 1 is used as the non-round component contour for this work, see figure 3a). A major degree of freedom of NCRT is the tip diameter of the tool d_{a0} . As a reference, there is also an analogy to ADRT here: Hosokawa et al. [17] studied the temperature of the tool flank using a fiber-coupled two-color pyrometer when turning AISI 304. Accordingly, the lowest temperature was achieved at $v_c/v_t \approx 1$. For NCRT, this means d_{a0} should be close to the reference diameter of the workpiece $d_{i2} = (d_{a2} + d_{i2})/2$ if assuming $i = 1$. The calculated reference tool contour is illustrated in figure 3b). In order to study the influence of d_{a0} on the surface, a smaller as well as a larger tool are designed in addition to the reference, see table 1. The feed rate f is adjusted to obtain a maximum chip thickness of $h_{max} = 50 \mu\text{m}$ in the reference.

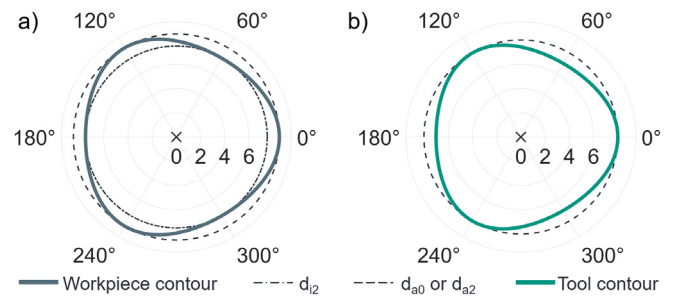


Figure 3: a) Workpiece contour. b) Reference tool contour ($d_{a0} = 16 \text{ mm}$).

The machining tests are carried out on a Traub TNL32-11 long automatic lathe (sliding headstock) under flood oil cooling. Coated carbide tools with individual contours manufactured by Hartmetall-Werkzeugfabrik Paul Horn GmbH are used. Parts with a total length of 50 mm are manufactured from brass (BR) and a titanium alloy (TI), see table 1. The manufactured surfaces are inspected at six positions ($0^\circ, 60^\circ, 120^\circ, 180^\circ, 240^\circ$ and 300°) with optical surface measuring device of type Nanofocus μSurf , see figure 3a). Surface roughness parameters are evaluated in the direction of feed motion. For the evaluation of the experimental data, the results of location A and B are summarized according to [18].

Table 1: Workpiece, tool and process parameters

Parameter	Value
d_R	18 mm
d_{a2}	17 mm
d_{i2}	15 mm
d_{i2}	16 mm
d_{a0}	12, 16, 20 mm
$\omega_0 = \omega_2$ ($i = 1$)	1,850 1/min
f (reference)	0.075 mm
Σ	90°
Material Brass	ASTM C38500 (CuZn39Pb3)
Material Titanium	ASTM F136 (Ti6Al4V ELI)

4. Results and Discussion

4.1. Simulation

Simulation reveals a strong dependence of the kinematic roughness Rz_{sim} on the location of the evaluation, see figure 4a). The extreme values occur at the intersection points of the workpiece contour with d_{a2} at 0° , 120° and 240° , as well as with d_{r2} at 60° , 180° and 300° , see figure 3a). Therefore these characteristic locations are marked with the labels A and B in the following. Regardless of f , Rz_{sim} is higher in area B than in area A. This is related to the different engagement conditions of the tool: In conventional turning, Rz is correlated with f and the corner radius of the turning tool r in good approximation [19], see equation 2. While larger tool radii are effective in area A, area B is created using smaller tool radii, see figure 3b). With increasing f , Rz_{sim} increases more strongly in area B, see figure 4b). This can also be attributed to the correlation according to equation 2. There is no dependence on the direction of tool rotation (DT, UT) in this respect.

$$Rz \sim \frac{f^2}{r} \quad (2)$$

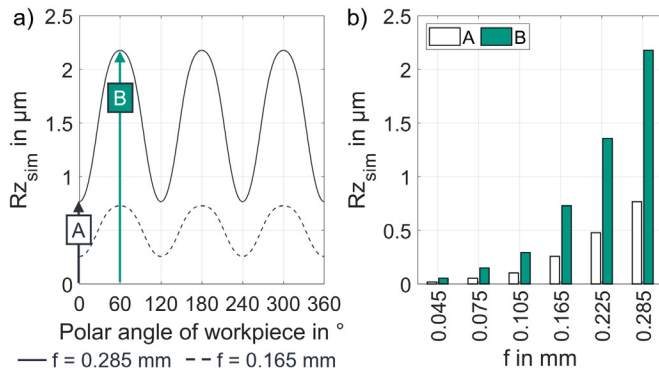


Figure 4: Calculated kinematic surface roughness R_{kin} ($d_{a0} = 16$ mm): a) Depending on the workpiece location. b) Depending on f .

Similar to Rz_{sim} , the calculated topography shows a strong dependence on the location, see figure 5. The theoretical texture of the surface follows the course of the contact line. It has a characteristic course for the process, according to which the contact point moves along the circumference of the workpiece along the longitudinal axis (Z-axis). Therefore, the angles at which the contact line intersects the workpiece axis also depends on the position.

In contrast to Rz_{sim} , the contact line shows a dependence on the direction of tool rotation (DT, UT), see figure 6a). The courses are opposite for the process variants, but intersect exactly at the points where the extreme values of Rz_{sim} occur. The contact lines can be found in the experiment in the area of the tool run-out on the workpiece. The opposite courses can clearly be distinguished, see figure 6b). For the investigated process, no dependence of the contact line on d_{a0} can be determined. This

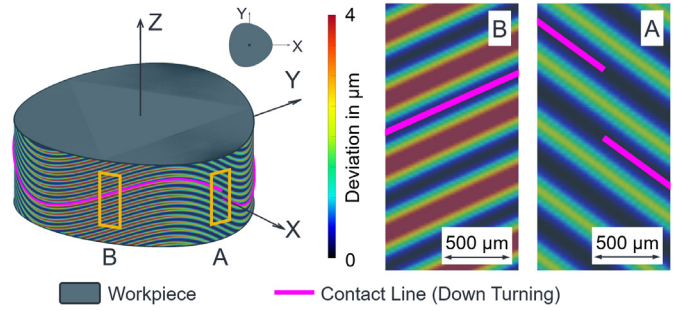


Figure 5: Calculated surface topography ($f = 0.5$ mm, $d_{a0} = 16$ mm).

suggests that the contact line depends only on the part contour for a given process kinematics.

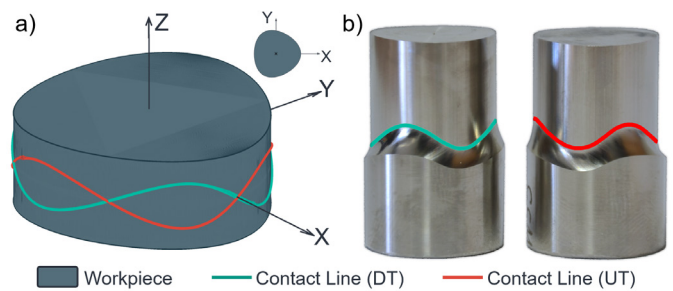


Figure 6: Comparison of contact lines depending on the direction of tool rotation ($f = 0.075$ mm, $d_{a0} = 16$ mm) : a) Simulation. b) Experiment.

4.2. Experimental Results

Similar to the simulation, increasing surface parameters with increasing f are also found in the experiment, see figure 7. In area B the values are also generally higher than in area A. Qualitatively, this confirms simulation. However, the measured values are dependent on the direction of tool rotation, with DT generally achieving the better surfaces. Besides, the absolute values of Rz and Rz_{sim} are very different, see figures 7c) and 4b).

For small f , the values differ by a factor of approx. 10. As f increases, the values become closer, so that in area B the difference drops to a factor of about 2. Comparable relations are also known for conventional turning, where model and experiment usually become congruent beyond a certain value of f . For this reason, kinematic-geometrical duplication is considered as a key factor for surface quality in conventional turning [20]. This does not apply for surfaces obtained by NCRT. With increasing f , the influence of kinematic-geometrical duplication increases, but overall the surface seems to be strongly influenced by other effects e.g. chip formation, material spring back and also dynamic aspects. This also explains the much smaller difference between areas A and B compared to the simulation.

The influence of d_{a0} also suggests that kinematic-geometrical duplication plays a rather minor role in terms of surface quality. Despite the fact that larger d_{a0} mean larger effective tool radii, for UT Ra increases with increasing d_{a0} , see

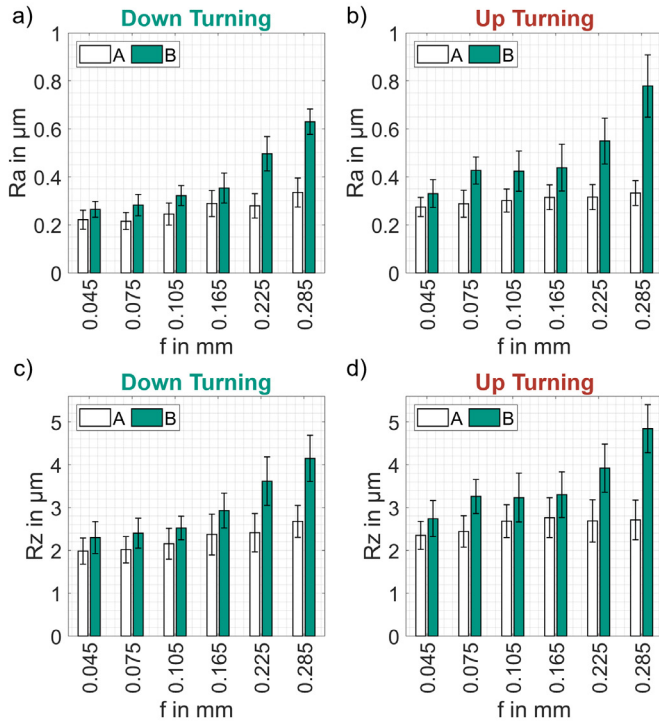


Figure 7: Experimental dependence of surface parameters on direction of tool rotation and f ($d_{a0} = 16$ mm, brass).

figure 8b). For DT, Ra is generally lower again. In contrast to UT, however, the reference tool diameter $d_{a0} = 16$ mm represents an optimum here, see figure 8a). For the small tool, Ra does not differ significantly in areas A and B.

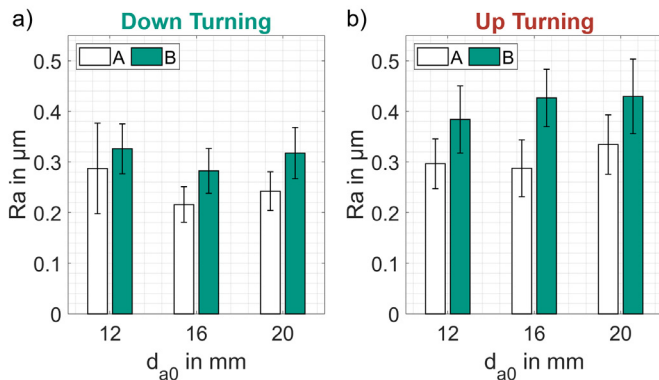


Figure 8: Experimental dependence of surface parameters on direction of tool rotation and d_{a0} ($f = 0.075$ mm, brass).

Figure 9 shows that the direction of tool rotation and d_{a0} do not only effect the surface parameters, but also strongly influence the obtained topography. Generally, cutting traces at an angle ζ to the direction of feed motion are visible on the workpiece surface. Therefore the topography is comparable with the ones obtained by ADRT [11]. In contrast to ADRT and in agreement with the simulation, ζ changes depending on the position, see figure 9a) and b). Different from the contact line, ζ does not change its direction from area A to B.

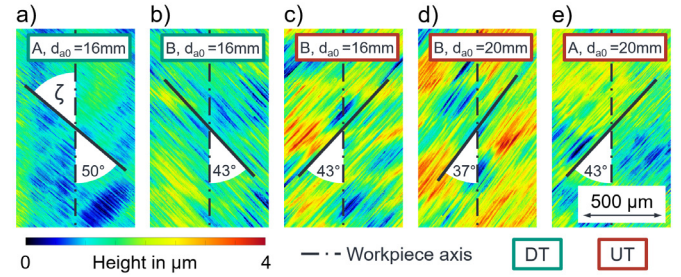


Figure 9: Experimental dependence of surface topography on direction of tool rotation and d_{a0} (brass).

However, reversal of the direction of ζ can be observed for the change in the direction of tool rotation, see figure 9c). The absolute value of ζ remains identical. At the same time, ζ depends on the tool diameter d_{a0} , see figure 9d). Accordingly, smaller ζ result for larger d_{a0} . This suggests that the topography is strongly dependent on the process-related sliding velocity of the tool tangential to the cutting edge in relation to v_c . For the investigated process, the sliding velocity corresponds to the rotation speed of the tool v_t . As both workpiece and tool have a non-circular contour, v_c and v_t are dependent on the location and therefore on d_a and d_i . Thus ζ can be calculated for the given process in areas A and B using equation 3. The calculated values then reflect the measured.

$$\tan(\zeta_A) = \frac{d_{a2}}{d_{i0}}, \quad \tan(\zeta_B) = \frac{d_{t2}}{d_{a0}} \quad (3)$$

In addition to the investigations in brass, components were also made from a titanium-alloy. Similar trends as described above can be seen with regard to the surfaces, see figure 10. While the values in area B increase, the values in area A tend to decrease slightly. This effect is more distinctive in downturning than in upturning. Thus, Ra in areas A and B differs less in the case of titanium than in the case of brass. This appears to push kinematic-geometrical duplication even further into the background when machining titanium with NCRT.

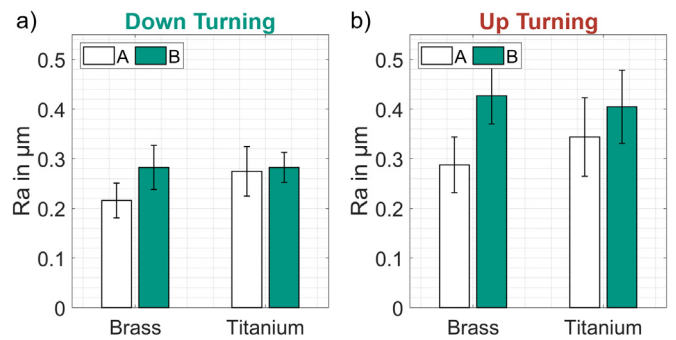


Figure 10: Experimental dependence of surface parameters on direction of tool rotation and workpiece material.

5. Conclusion

In this work the novel process Non-Circular-Rotary-Turning (NCRT) was presented and the surfaces obtained were basically investigated. Therefore, a dixel-based simulation model was utilized to study the kinematic nature of the surfaces depending on the process parameters. In experimental investigations it could be shown that the process generally works and surfaces with good finish could be produced. The following conclusions can be drawn in summary:

- Better surfaces are generally achieved in downturning. Surface finishes of $R_a \leq 0.3 \mu\text{m}$ can be obtained when machining brass or titanium. As for conventional turning, the surface parameters become worse as the feed rate increases.
- Due to the non-circular contour of component and tool, the surface quality depends on the location on the workpiece. The simulation is able to determine the locations of the best and worst expected surface quality.
- The measured surface roughness deviates strongly from the simulated values. This suggests that the kinematic-geometric duplication plays a rather secondary role for surface finish obtained by NCRT.
- Cutting traces form at an angle to the direction of feed motion. Their appearance differs significantly from simulation. The angle is strongly influenced by the process-related sliding velocity of the tool tangential to the cutting edge. Therefore, it is affected by the diameter of the tool. The orientation of the angle changes with the change of the direction of tool rotation.
- The contact line gives information about the shape of the tool run-out. It is not influenced by the tool diameter but on the direction of tool rotation.
- Due to its kinematics and the non-circular contour of tool and workpiece, the process is characterized by strong local and temporal changes of the cutting conditions. Future work should deal with the relations to workpiece quality in terms of surface finish and geometry.

Acknowledgment

The research presented was funded by the German Federal Ministry of Education and Research (BMBF) within the Framework Concept “Production for medical technology - economical and of the highest quality (ProMed)” and managed by the Project Management Agency Karlsruhe (PTKA). The authors would like to thank the Ministry of Science, Research and Arts of the Federal State of Baden-Württemberg for the financial support of the projects within the InnovationsCampus Future Mobility (ICM). The authors are responsible for the contents of this publication.

References

- [1] Maximov, J. (2005), A new method of manufacture of hypocycloidal polygon shaft joints, *Journal of Materials Processing Technology*, vol. 166, pp. 144–149.
- [2] Leidich, E., Reiß, F. and Schreiter, R. (2017), Investigations of hypocycloidal shaft and hub connections, *Materialwissenschaft und Werkstofftechnik*, vol. 48, pp. 760–766.
- [3] Maximov, J. and Hirstov, H. (2005), Machining of hypotrochoidal surfaces by adding rotations around parallel axes, part 1: Kinematics of the method and rational field of application, *Trakya University Journal of Natural Sciences*, vol. 6, pp. 1–11.
- [4] Wu, D., Zhao, T., Chen, K. and Wang, X. (2009), Application of active disturbance rejection control to variable spindle speed noncircular turning process, *International Journal of Machine Tools and Manufacture*, vol. 49, pp. 419–423.
- [5] Yang, J., Ai, W., Liu, Y. and Chen, B. (2018), Kinematics model and trajectory interpolation algorithm for CNC turning of non-circular profiles, *Precision Engineering*, vol. 54, pp. 212–221.
- [6] Wu, D. and Chen, K. (2010), Chatter suppression in fast tool servo-assisted turning by spindle speed variation, *International Journal of Machine Tools and Manufacture*, vol. 50, pp. 1038–1047.
- [7] Hühsam, A. (2002), Modellbildung und experimentelle Untersuchung des Wälzschälens, Forschungsberichte aus dem Institut für Werkzeugmaschinen und Betriebstechnik der Universität Karlsruhe (wbk), Dissertation.
- [8] Uhlmann, E., Kaulfersch, F. and Roeder, M. (2014), Turning of high-performance materials with rotating indexable inserts, *Procedia CIRP*, vol. 14, pp. 610–615.
- [9] Shaw, M., Smith, P. and Cook, N. (1952), The Rotary Cutting Tool, *Transactions of the ASME*, pp. 1065–1076.
- [10] Nakajima, H., Kato, A., Sasahara, H., Yamamoto, H., Muraki, T. and Tsutsumi, M. (2008), Effect of Rotary Cutting Tool Posture on Machining Performance utilizing Multi-Tasking Lathe, *Journal of Advanced Mechanical Design, Systems, and Manufacturing*, vol. 4, pp. 532–539.
- [11] Olgun, U. and Budak, E. (2013), Machining of Difficult-to-Cut-Alloys Using Rotary Turning Tools, *Procedia CIRP*, vol. 8, pp. 81–87.
- [12] Kaulfersch, F. and Roeder, M. (2013), Cutting of Nickel-Based Superalloys with Rotating Indexable Inserts, *Advanced Materials Research*, pp. 116–123.
- [13] Joch, R., Sajgalik, M., Czan, A., Holubjak, J., Cedzo, M. and Cep, R. (2022), Effects of Process Cutting Parameters on the Ti-6Al-4V Turning with Monolithic Driven Rotary Tool, *Materials*, vol. 15, pp. 1–13.
- [14] Hilligardt, A., Klose, J. and Schulze, V., OpenSkiving [Software], version 1.3, <https://openskiving.kit-campus-transfer.de/>, accessed 2 November 2021.
- [15] Hilligardt, A., Böhlend, F., Klose, J., Gerstenmeyer, M. and Schulze, V. (2021), A new approach for local cutting force modeling enabling the transfer between different milling conditions and tool geometries, *Procedia CIRP*, vol. 102, pp. 138–143.
- [16] Arndt, T., Sellmeier, V. and Schulze, V. (2023), Model-based tool design for the manufacturing of hypocycloidal internal profiles by polygon turning, *Procedia CIRP*, vol. 117, pp. 7–12.
- [17] Hosokawa, A., Ueda, T., Onishi, R., Tanaka, R. and Furumoto, T. (2010), Turning of difficult-to-machine materials with actively driven rotary tool, *CIRP Annals Manufacturing Technology*, vol. 59, pp. 89–92.
- [18] Rudmin, J. (2010), Calculating the exact pooled variance, *Physics Department, James Madison University, Harrisonburg*.
- [19] Vajpayee, S. (1981), Analytical study of surface roughness in turning, *Wear*, vol. 70, pp. 165–175.
- [20] He, C., Zong, W. and Zhang, J. (2018), Influencing factors and theoretical modeling methods of surface roughness in turning process: State-of-the-art, *International Journal of Machine Tools and Manufacture*, vol. 129, pp. 15–26.